



Contents lists available at ScienceDirect



Applied Catalysis A: General

journal homepage: www.elsevier.com/locate/apcata

Photocatalytic water splitting and hydrogenation of CO₂ in a novel twin photoreactor with IO₃⁻/I⁻ shuttle redox mediator

Sheng-Hung Yu^a, Cheng-Wei Chiu^a, Yi-Ting Wu^a, Chi-Hung Liao^a, Van-Huy Nguyen^{a,b}, Jeffrey C.S. Wu^{a,*}

^a Department of Chemical Engineering, National Taiwan University, Taipei 10617, Taiwan

^b Department of Chemical Engineering, National Taiwan University of Science and Technology, Taipei City 106, Taiwan

ARTICLE INFO

Article history:

Received 17 June 2015

Received in revised form 20 August 2015

Accepted 22 August 2015

Available online xxx

Keywords:

Twin photoreactor

Photoreduction

CO₂

Hydrogenation

Water splitting

ABSTRACT

One of the major drawbacks in photoreduction of carbon dioxide (CO₂) into hydrocarbons is the high thermodynamic barrier involved, resulting in low photoreduction quantum efficiency (PQE). A novel twin photoreactor system has been developed to enhance the QE of CO₂ reduction as a solution to this limitation. The twin photoreactor divides the oxygen (O₂)-generating photocatalyst and the dual-function photocatalyst having both CO₂ reduction and hydrogen (H₂) production capabilities in two compartments by a membrane thus preventing the undesired reverse reaction. Herein, the dual-function photocatalyst can hydrogenate CO₂ via the produced H₂, allowing the overall reaction to be more thermodynamically favorable. The charge balance was accomplished by the aid of IO₃⁻/I⁻ redox mediator in the twin photoreactor for shuttling electrons. Two visible-light photocatalysts, Pt/WO₃ (O₂-generating photocatalyst) and GaN:ZnO-Ni/NiO (both CO₂-reducing and H₂-generating photocatalysts) were used. We found out that through the application of the twin photoreactor system under artificial sunlight (AM1.5G 300 W Xenon lamp), the QE was enhanced more than 4-folds in comparison with that in the single photoreactor, an increase from 0.015% to 0.070%. A possible enhancing mechanism for twin photoreactor, in compare with the conventional single photoreactor, is also proposed based on the knowledge of species present during the photocatalytic reaction.

© 2015 Elsevier B.V. All rights reserved.

1. Introduction

Global warming and energy crisis have become the most concerned global challenges in the 21st century. Since the industrial revolution, the emission of carbon dioxide (CO₂) into the atmosphere has risen rapidly throughout the years, along with that of other greenhouse gases, is cited as one of the major causes of global warming [1]. On the other hand, the usage of conventional fossil fuels has gradually led to resource depletion and environmental pollution [2]. Recently, a popular idea towards artificial photosynthesis was proposed which considered CO₂ as a potential building block for the development of alternative energy [3]. If this strategy were succeeded, sustainable economic and environmental development may be realized.

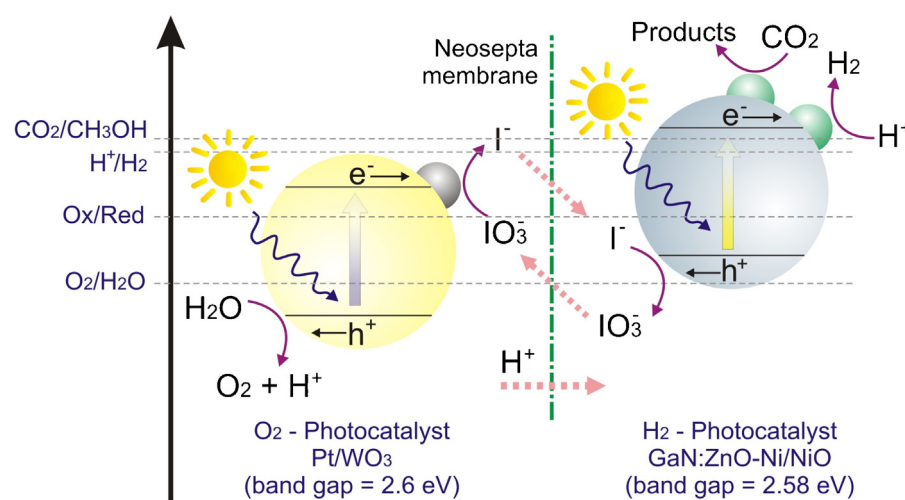
In 1979, Inoue et al. had firstly conducted several CO₂ experiments in a slurry batch reactor by using WO₃, TiO₂, ZnO, CdS, GaP, and SiC photocatalysts [4]. After years of research, a revolutionized

technology has been developed, that is, the use of photocatalyst in the reduction of CO₂ into renewable hydrocarbons such as methane (CH₄), methyl formate, methanol (CH₃OH), etc. [3,5,6]. It is worth mentioning that the presence of hydrogen (H₂) can significantly improve the yield of hydrocarbons [7–10]. This is due to the fact that hydrogenation by H₂ is more favorable than by H₂O in the reduction of CO₂. However, adding fossil-H₂ directly for CO₂ hydrogenation is not a practical way because more CO₂ would be produced by reforming of fossil fuels. Looking forward with a more practical route, to develop a solar-H₂ is necessary for providing the H₂ needed in CO₂ hydrogenation [11].

One of the most promising ideas for solar H₂ is to apply Z-scheme water splitting driven by IO₃⁻/I⁻ shuttle redox mediator [12], then perform CO₂ hydrogenation in the photoreactor system. Our group recently reported that a twin photoreactor based on the dual photocatalytic system, which consists of H₂- and O₂-generating photocatalysts divided by a membrane. The main advantage of Z-scheme is that H₂ and O₂ can be separately produced [13]. As shown in Scheme 1, in the right-hand side, proton is reduced to hydrogen by photo-excited electrons and CO₂ can be hydrogenated to hydrocarbons at the same time, while I⁻ is oxidized to IO₃⁻ by holes. In

* Corresponding author. Fax: +886 2 23623040.

E-mail address: cswu@ntu.edu.tw (J.C.S. Wu).



Scheme 1. The diagram of combined H_2O water splitting and CO_2 photo-hydrogenation by a Z-scheme system.

the left-hand side, the photo-excited electrons reduce IO_3^- back to I^- , while water is oxidized to O_2 by holes. The proton generated in the left-hand side is diffused to the right-hand side due to concentration gradient. The redox mediators, I^-/IO_3^- , are circulated between two sides via the Neosepta membrane. As shown in Eqs. ((1)–(4)), after the reduction and oxidation of the redox mediators, IO_3^- and I^- are counter-diffused toward the counter sides due to the concentration gradients caused by the photoreaction. Thus through this cycle, the mass and charge balances are maintained when the generations of O_2 and hydrocarbons are carried out simultaneously in each side.

1.1. Oxidation of I^-



1.2. Reduction of IO_3^-



Scheme 2 shows the schematics of twin photoreactor, which consists of IO_3^-/I^- as shuttle redox mediator. There are several advantages in the twin photoreactor system. Firstly, CO_2 could be directly hydrogenated to hydrocarbons by the produced H_2 . Secondly, the separation of H_2 and O_2 prevents the backward reaction of water splitting and the oxidation of the produced hydrocarbons by O_2 back into CO_2 . Thirdly, with the aid of IO_3^-/I^- shuttle redox mediator, more electron transfer can be achieved as compared to the $\text{Fe}^{3+}/\text{Fe}^{2+}$ system [13]. Last but not least, the neutral condition of I^-/IO_3^- , with an anion-exchanged membrane, could dissolve more CO_2 into the reacting solution, leading to higher product yield as compared to the acidic condition of $\text{Fe}^{3+}/\text{Fe}^{2+}$.

Numerous investigators have reported that the photocatalytic reduction of CO_2 in the presence of H_2 proceeds over many simple oxides such as MgO [7], ZrO_2 , [14], ZnO [15], and Ga_2O_3 [16,17]. It is interesting that $(\text{Ga}_{1-x}\text{Zn}_x)(\text{N}_{1-x}\text{O}_x)$, which is typically synthesized by nitriding a mixture of Ga_2O_3 and ZnO powders, is also potentially applicable in water splitting [18–20]. In order to enhance efficiency of overall water splitting on $(\text{Ga}_{1-x}\text{Zn}_x)(\text{N}_{1-x}\text{O}_x)$ photocatalyst, loading with Ni/NiO has attracted considerable interest [21]. When Ni particles are reoxidized at 473 K, its shell become NiO can effectively prevent the loss of products for the reverse

reaction from H_2 and O_2 into H_2O [21,22]. In brief, it is reasonable to develop $\text{GaN:ZnO-Ni}/\text{NiO}$ photocatalyst for CO_2 hydrogenation through overall water splitting. First, H_2O is split into H_2 and O_2 via the water splitting. Then, the generated H_2 is directly used to perform the CO_2 photo-hydrogenation to design products. In regard to the photocatalyst for O_2 -generating, WO_3 is found as the most attractive candidate with high and stable photocatalytic activity [13]. To further improve the efficiency of photocatalyst, Pt-loaded WO_3 , which facilitates the separation of photo-generated electrons and holes by trapping electrons, is also considered.

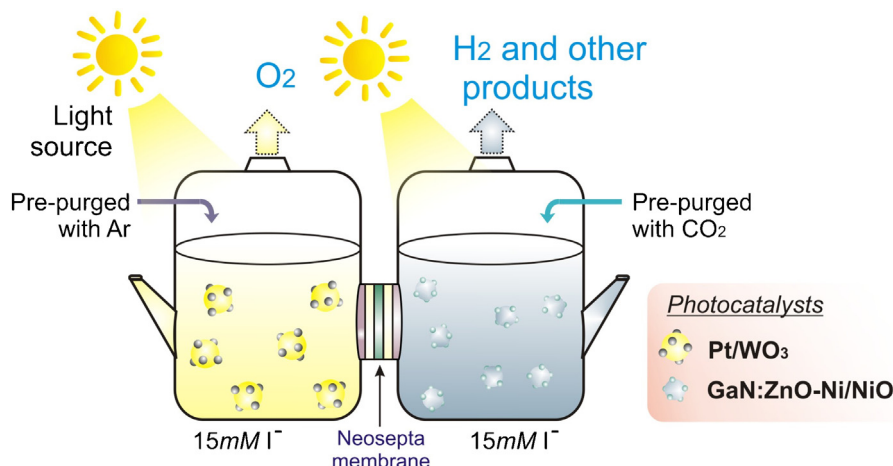
This study proposes the combined H_2O water splitting and CO_2 hydrogenation in the twin photoreactor with IO_3^-/I^- shuttle redox mediator, which is a highly promising process for photocatalytic reduction of CO_2 . Based on the knowledge of species present during the photocatalytic reaction, a possible photo-activity enhancing mechanism for the twin photoreactor is also proposed in comparison with the conventional single photoreactor.

2. Experimental

2.1. Preparation of photocatalysts

GaN:ZnO catalyst was prepared by heating a mixture of 2.16 g $\beta\text{-Ga}_2\text{O}_3$ (Acros, 99.99%) and 1.88 g ZnO (J.T. Baker 99%) at 1125 K for 15 h under NH_3 flow [20]. Prior to the nitridation process, $\beta\text{-Ga}_2\text{O}_3$ and ZnO were pulverized in a mortar for 30 min. After the nitridation process, the resulting powder was pulverized for another 30 min. For the final step, GaN:ZnO was calcined under air flow at 873 K for 2 h. $\text{GaN:ZnO-Ni}/\text{NiO}$ catalyst was prepared by incipient wetness impregnation as described previously [23]. Firstly, 0.3 g of GaN:ZnO powder was impregnated with 3–4 mL of de-ionized water containing 2.5 wt.% of Ni precursor ($\text{Ni}(\text{NO}_3)_2 \cdot 6\text{H}_2\text{O}$, Nacalai Tesque Inc.) over an evaporating dish. After that, the slurry was placed in an oven at 353 K to ensure complete dryness. Lastly, the resulting powder was reduced with H_2 for 2 h at 573 K and then oxidized by air for 1 h at 473 K to form a core-shell structure of Ni/NiO cluster.

Pt/WO_3 catalyst was prepared by a photo-deposition process. Firstly, H_2PtCl_6 solution of desired concentration was mixed with commercial WO_3 (Aldrich 99.995%) powder to give a 0.5 wt.% of Pt-loaded. The well-mixed solution was next irradiated by UV lamp with an intensity of 5 W/cm^2 for 1.5 h to perform the photo-deposition process. The resulting powder was subsequently washed by de-ionized water and centrifuged several times to ensure that there was no residual Cl^- remaining on the photocata-

**Scheme 2.** The diagram of a novel twin photoreactor system.

lyst. Lastly, the washed photocatalyst was dried in an oven at 353 K to obtain Pt/WO₃.

2.2. Characterization of photocatalysts

The crystalline of photocatalysts was analyzed by Rigaku M03XHF Ultima IV X-ray diffractometer (XRD) in the diffraction angle (2θ) between 10° and 80°, using Cu-K α radiation as the X-ray source. The X-ray (wavelength $\lambda = 1.5418 \text{ \AA}$) tube equipped with a copper target was operated at 40 mA and 40 kV. The UV-vis absorption spectrum of photocatalysts was measured by the UV-vis spectrometer (Varian Cary-100) in the wavelength range between 200 and 800 nm. Field emission scanning electron microscopy (FE-SEM) was carried out on a JEOL JSM-7000 FE-SEM. The photocatalysts were sputtered with a thin layer of Pt film to prevent surface charging. The morphology of Pt/WO₃ photocatalyst was observed by Philips FEI Tecnai F20 G² high-resolution transmission electron microscope (HR-TEM) at an acceleration voltage of 200 kV. The specimen was prepared by ultrasonically dispersing the sample into ethanol, depositing droplets of the suspensions onto a copper mesh (200 meshes), and keeping 24 h in a vacuum dry oven (DOV30). For surface analysis, X-ray photoelectron spectroscopy (XPS) was conducted to identify the composition and chemical status of photocatalysts by the Theta Probe XPS (Thermo Scientific) with Mg target as the X-ray source of 1253.6 eV.

2.3. Counter-diffusion of Neosepta membrane

The Neosepta membrane (TAIYEN Company, Taiwan) was used in this experiment as an anion-exchanged membrane for the counter-diffusion of I⁻ and IO₃⁻ ions in the twin photoreactor. The membrane was pretreated by immersing it into the same concentration of NaI solution under which the photocatalytic reaction was performed. A concentration of 10 mM NaI or NaIO₃ solution was placed in the counterpart compartment of the twin photoreactor separated by Neosepta membrane to evaluate the ion transfer rates and the diffusivities of I⁻ and IO₃⁻. The concentrations of I⁻ and IO₃⁻ were measured in each compartment with ion chromatography (ICS-1000) after several hours of diffusion, and the results of ion transfer rates and diffusivities were summarized in Table 1. The transfer rates of I⁻/IO₃⁻ redox mediators through the membrane were found to be much higher than the reaction rate of the CO₂ reduction, suggesting that the reaction rate would not be constrained during the photocatalytic reaction.

Table 1
The diffusion of iodide and iodate ions through Neosepta membrane.

Ion species	Apparent diffusivity (cm ² s ⁻¹)	Ion transfer rate under 10 mM conc. Difference (μmol h ⁻¹)
I ⁻	9.0 × 10 ⁻⁷	24.77
IO ₃ ⁻	7.4 × 10 ⁻⁷	20.37

2.4. CO₂ photoreduction in a twin and a single batch photoreactor system

For the CO₂ photoreduction reaction in the twin photoreactor, Pt/WO₃ (0.3 g) and GaN:ZnO-Ni/NiO (0.3 g) photocatalysts were placed in the counterpart compartments separated by the circular Neosepta membrane (TAIYEN Co.). Then, de-ionized water (200 mL) combined with NaI (15 mM) was added in each compartment, as shown in Scheme 2. That the reason 15 mM of I⁻ was selected to carry out the subsequent CO₂ reduction is mentioned in the Supplementary material. Prior to the photocatalytic reaction, the left and right compartments were purged with ultra-pure Ar gas and ultra-pure CO₂ for 30 min, respectively, to remove residual air in both compartments and to introduce CO₂ into the right compartment for the reaction. During the photo-reaction, the solution in each compartment was stirred and irradiated with an artificial sunlight (AM1.5G 300 W Xenon lamp, 100 mW cm⁻²) that has the same power and spectral distribution of the sun at 48.5° zenith angle.

The produced O₂ and H₂ were collected separately in each compartment every 1 h with an on-line sampling loop (1 mL) connected to a thermal conductivity detector (China GCTCD 2000) for analysis. A molecular sieve 5 Å packed column of length 3.5 m was installed, and ultra-pure Ar was used as carrier gas in the GC-TCD for high sensitivity of H₂. For the detection of hydrocarbons in the right-hand compartment, liquid samples (1–10 μL) were withdrawn and injected into the flame ionization detector (China GC-FID 9800) after filtering the photocatalyst. To further improve the CO detection limit, a methanizer packed with Ni catalyst was connected to GC-FID to convert CO into CH₄ with H₂ at 633 K. A Porapak Q column of length 2 m was installed, and pure N₂ was used as the carrier gas for FID in the detection of hydrocarbons.

For comparison, the CO₂ photoreduction reaction was also performed in a single photoreactor. At first, GaN:ZnO-Ni/NiO (0.3 g) photocatalyst was placed in a quartz photoreactor filled in de-ionized water (180 mL) with 0.2 M NaOH. Then, the solu-

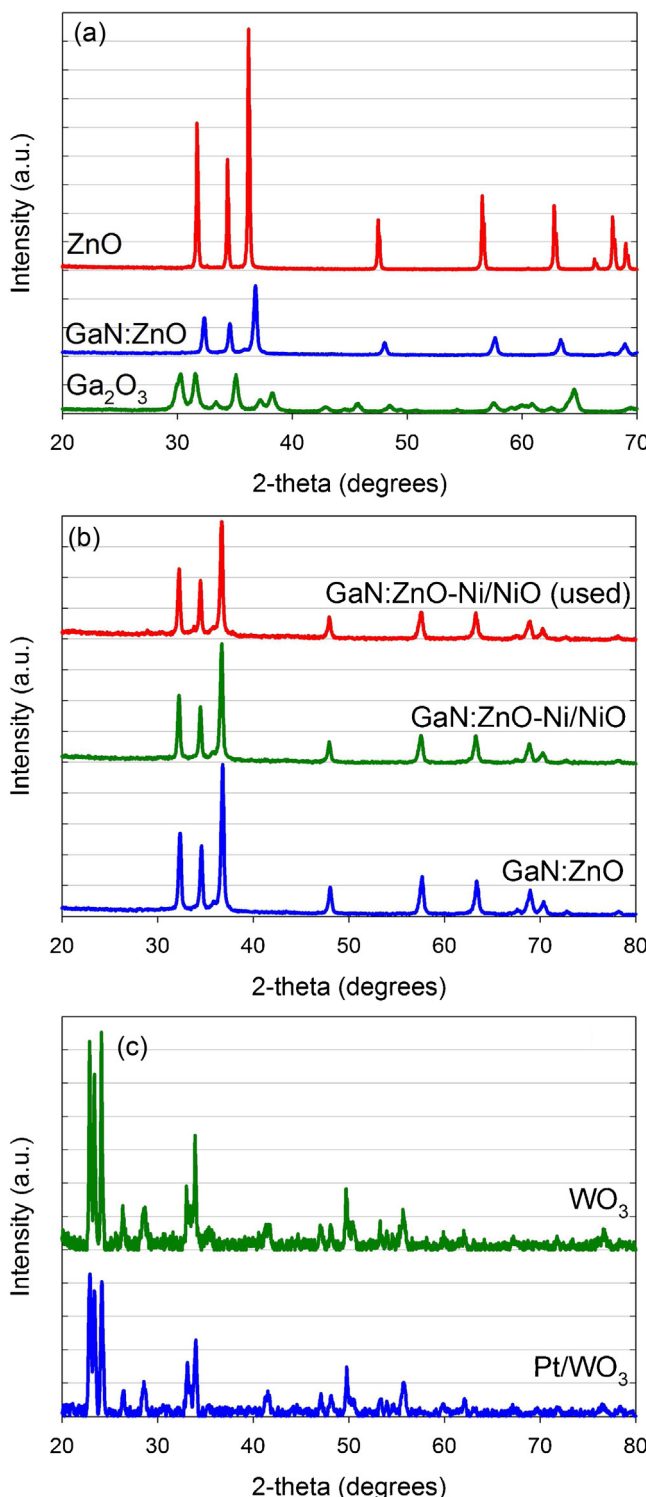


Fig. 1. XRD patterns of photocatalysts: (a) GaN:ZnO in compared with starting materials of ZnO and Ga₂O₃; (b) GaN:ZnO in compared with fresh and spent GaN:ZnO-Ni/NiO; (c) commercial WO₃ and Pt/WO₃.

tion was purged with pure CO₂ for 30 min before performing the photocatalytic reaction under visible-light (300W Xenon lamp, 270 mW cm⁻²). The liquid samples (1–10 μL) and gas samples (0.5–1 mL) were analyzed by GC-FID for the detection of hydrocarbons in both aqueous and gas phases.

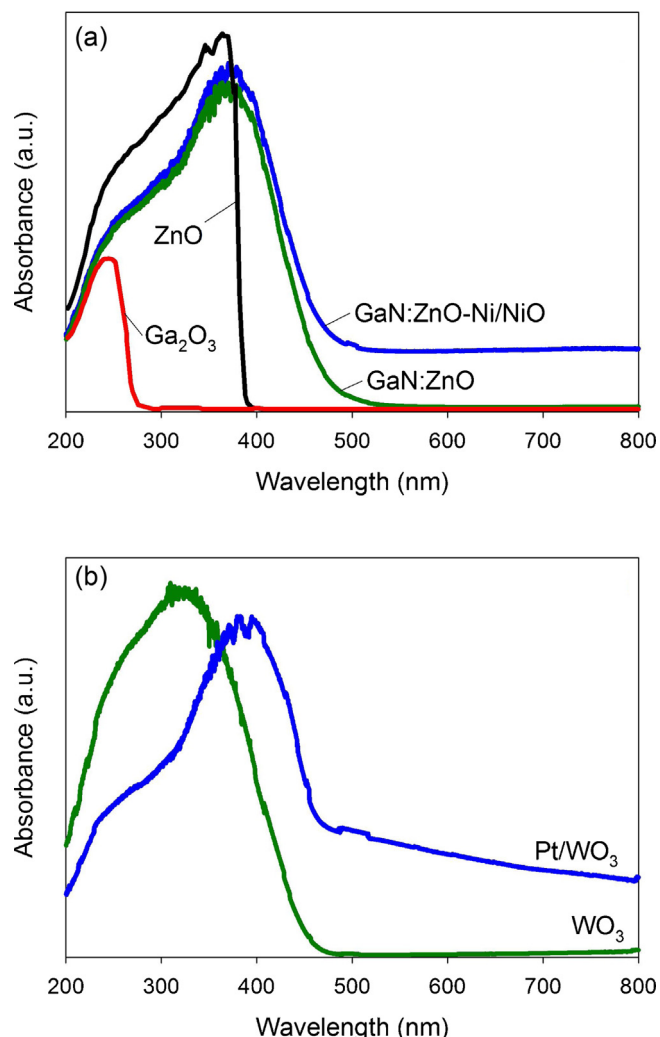


Fig. 2. UV-vis spectra of photocatalysts: (a) ZnO, Ga₂O₃, GaN:ZnO, and GaN:ZnO-Ni/NiO; and (b) WO₃, and Pt/WO₃.

3. Results and discussion

3.1. Characterization of photocatalyst

Fig. 1 depicts the X-ray diffraction (XRD) patterns of all photocatalysts and their references. In details, **Fig. 1a** reveals patterns of the prepared GaN:ZnO sample and its precursors of β-Ga₂O₃ and ZnO. Clearly, the position of the *d*(100) diffraction peak of GaN:ZnO shifted slightly to higher angles (2-theta), in comparison with that of ZnO. Moreover, no peaks can be assigned to either Ga₂O₃ or ZnO, indicating that complete nitridation of the precursors was achieved by nitriding a mixture of β-Ga₂O₃ and ZnO at 1125 K for 15 h. This phenomenon is consistent with that observed in previous studies [19,20]. There is no noticeable change in their XRD patterns before and after loading the Ni/NiO as co-catalysts, (**Fig. 1b**), suggesting that Ni/NiO co-catalysts did not change the structure of bulk. However, the presence of Ni/NiO co-catalyst slightly reduces the GaN:ZnO crystallites. All the peaks of GaN:ZnO have intensity higher than that of GaN:ZnO-Ni/NiO. Additionally, we also observed no change in the XRD pattern of GaN:ZnO-Ni/NiO after 8 h of reaction, indicating that this photocatalyst was essentially stable in the reaction. **Fig. 1c** shows that the XRD pattern of WO₃ which is similar to that of orthorhombic WO₃ (JCPDS file 20-1324) [13]. Obviously, the peaks of Pt are not detected, showing that Pt loading is very small and highly dispersed on the WO₃ surface.

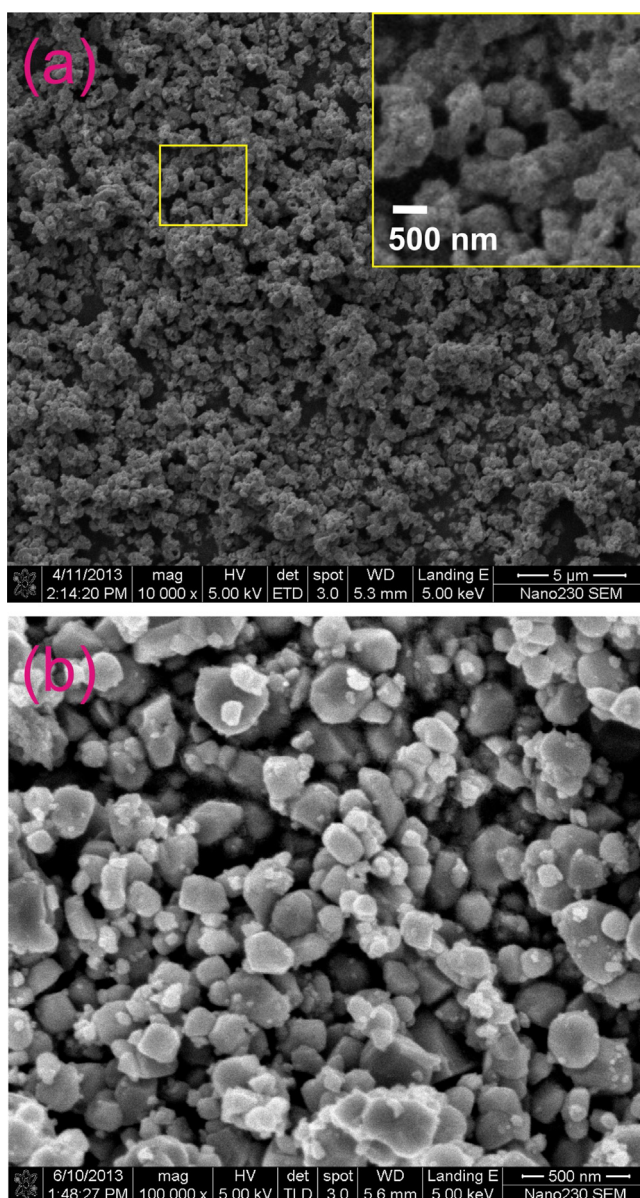


Fig. 3. FE-SEM images of photocatalysts: (a) GaN:ZnO and (b) WO₃.

Regarding the light harvesting, the optimal photocatalyst is expected to absorb light efficiently over the whole wavelength range of the solar spectrum. Fig. 2 shows the UV-vis absorption spectra of all samples, such as Ga₂O₃, ZnO, GaN:ZnO, GaN:ZnO-Ni/NiO, WO₃ and Pt/WO₃ photocatalysts. Obviously, the absorption edge of GaN:ZnO after the nitridation process is at longer wavelengths than those of starting materials Ga₂O₃ and ZnO, which are only active in the ultraviolet region. As suggested from the previous study [18], the visible light response of GaN:ZnO comes from the repulsion between N2p and Zn3d orbitals. It is noted that both two photocatalysts GaN:ZnO-Ni/NiO and Pt/WO₃ are active in the visible-light region up to 500 and 480 nm, respectively. With the presence of Ni/NiO, a slightly shift of the absorption edge to longer wavelengths with a gradual increase in absorption can be observed. On the other hand, the significant red-shift in absorption edge over Pt/WO₃ is attributed to the Pt loading. The scattering of photons by crystal defects created upon metal-loaded and the free carrier absorption of photons contribute to the shift of the absorption edge and the enhancement of absorption [24].

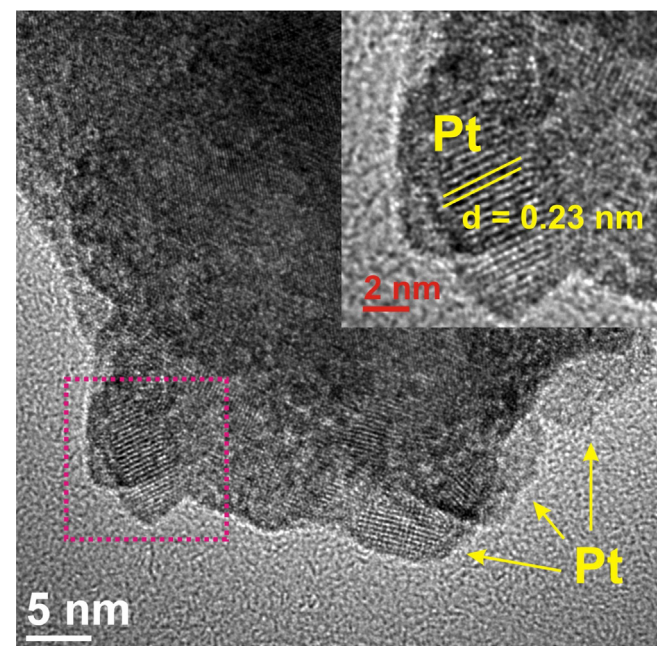


Fig. 4. HR-TEM image of Pt/WO₃ photocatalyst.

To evaluate the morphology of GaN:ZnO and WO₃ photocatalysts, the FE-SEM analysis was performed, as shown in Fig. 3. The particles of GaN:ZnO sample are uniform, and the average particle size is around 400–600 nm. On the other hand, the mean particle size of WO₃ is about 200–400 nm. The morphology of Pt/WO₃ photocatalyst was further characterized by transmission electron microscopy (TEM). Fig. 4 clearly shows that a number of tiny Pt nano-particles are well dispersed on the WO₃ surface. Furthermore, the Pt nano-particles have spherical or hemispherical shape; their particle size is about 4–7 nm. The lattice fringe (inset, Fig. 4) with $d = 0.23 \text{ nm}$ is corresponded to Pt (111) (JCPDS file 65-2868, $d = 0.227 \text{ nm}$). The TEM observation is in accordance with the XRD results.

Further evidence of co-catalysts loaded on the prepared photocatalysts was observed through the XPS analysis. Fig. 5a exhibits the Ni 2p spectrum of Ni/NiO-loaded GaN:ZnO. After curve fitting, the spectrum of Ni 2p can be divided into two pairs of peaks. In details, peaks at 858.0 and 874.6 eV are corresponding to Ni 2p_{3/2} and Ni 2p_{1/2}, respectively, while peaks at 867.8 and 880.4 eV are assigned to Ni satellite [25]. Fig. 5b reveals the Pt 4f spectrum of Pt-loaded WO₃. As expected, the principal peaks are attributed to Pt⁰ at 70.9 eV (4f_{7/2}) and 74.2 eV (4f_{5/2}) [26]. It suggests that all Pt ions are completely reduced by the photo-deposition process.

3.2. Photocatalytic CO₂ reduction

3.2.1. Blank test

Table 2 shows the result of blank experiments, which are conducted before performing the photocatalytic reaction to prove that the formation of the product (hydrocarbons, H₂) actually comes from photoreduction and not from CO₂ contaminations or the photocatalyst itself. Argon was purged into the reacting solution to bring out any impurity contained within. Note that a carbon source is needed to be reduced into hydrocarbons. There are two possible sources: (1) the impurity from the reaction system, and (2) the carbon residue on the photocatalyst. For the first blank experiment (Entry 1, Table 2), CO₂ was not purged into the reacting system, resulting in no product generated even with the presence of the photocatalyst and light irradiation. This proves that both the reaction system and the photocatalyst contain a minimal contamination

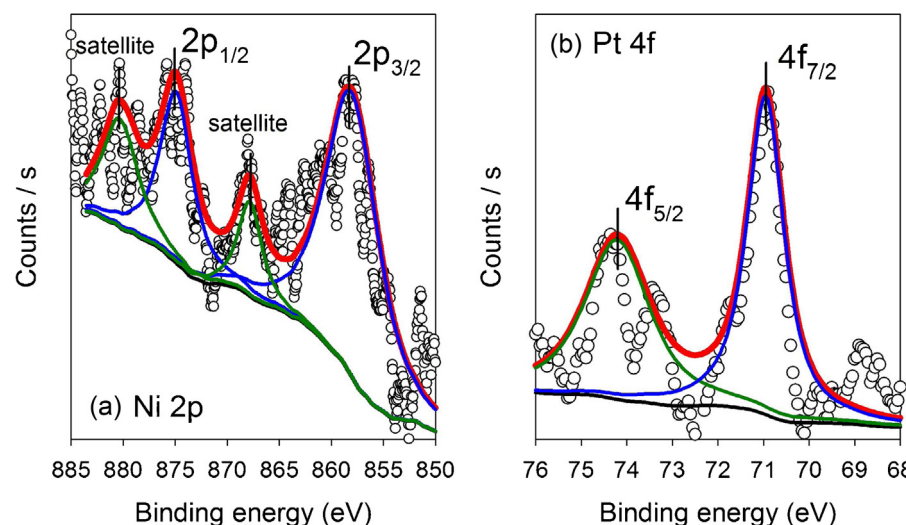


Fig. 5. XPS spectra: (a) Ni 2p of Ni/NiO loaded on GaN:ZnO and (b) Pt 4f of Pt/WO₃ photocatalysts.

Table 2

The result of blank experiment for slurry batch reaction.

Entry	Experimental conditions				Products ($\mu\text{mol g}_{\text{cat}}^{-1} \text{ h}^{-1}$)
	Ar	CO ₂	Catalyst	Light source	
1	O	X	O	O	BDL
2	O	O	X	O	BDL
3	O	O	O	X	BDL

Light source: 300 W Xenon lamp 270 mW cm⁻².

Abbreviations: X—absent in the photoreactor; O—present in the photoreactor; BDL—below detection limit of gas chromatography.

Table 3

The Enthalpy (ΔH°) and Gibbs free energy (ΔG°) values changes in some reactions.

Eqs.	Reactions	ΔH° (kJ mol ⁻¹)	ΔG° (kJ mol ⁻¹)
(5)	CO ₂ (g) + 3H ₂ (g) → CH ₃ OH (l) + H ₂ O (l)	-137.8	-10.7
(6)	CO ₂ (g) + 4H ₂ (g) → CH ₄ (g) + H ₂ O (l)	-259.9	-132.4
(7)	CH ₄ (g) + ½ O ₂ (g) → CO (g) + 2H ₂ (g)	-59.7	-86.5
(8)	2CO (g) + O ₂ (l) → 2CO ₂ (g)	-283.2	-257.3
(9)	CO (g) + H ₂ (l) → HCHO (l)	-5.5	27.3
(10)	CO (g) + 2H ₂ (g) → CH ₃ OH (l)	-131.6	-29.9

Aspen was used in calculating the ΔH° and ΔG° data [27].

that is too small to be detected by GC. Additionally, the photocatalyst itself contains nearly no carbon residue because its synthesis process did not use any carbon-containing precursor. There are also three essential elements in performing the photocatalytic reaction, including (1) CO₂, (2) photocatalyst and (3) light source. Clearly, with any of these parts missing, no product could be detected.

3.2.2. Single photoreactor

Photocatalysts were first screened for their photocatalytic CO₂ reduction activity by using a single photoreactor under visible-light (300 W Xenon lamp, 270 mW cm⁻²). We found that GaN:ZnO-Ni/NiO was a dual-function photocatalyst with both CO₂-reducing and H₂-generating capability. In details, CH₃OH was found as the main product. A total of 18.96, 2.08, 13.44, 1.87 and 0.43 $\mu\text{mol g}_{\text{cat}}^{-1}$ of H₂, CH₄, CH₃OH, formaldehyde (HCHO) and CO, respectively, were produced over 6 h of photo-reaction. Table 3 summarizes some possible reaction paths with their ΔH° and ΔG° values involved in CO₂ hydrogenation [27]. Most exothermic reactions ($\Delta H^\circ < 0$) are thermodynamically favorable with negative ΔG° values. The correlation between the amount of H₂, CO, and CH₄ produced and the reaction over GaN:ZnO-Ni/NiO photocatalyst are presented in Fig. 6. The photocatalyst produces H₂ monoton-

ically, while both CO and CH₄ yields increase initially in the first 2–3 h, and then decrease dramatically as reaction time goes on. This can be understood by considering the back reaction of O₂. Due to the presence of O₂ producing during the photocatalytic reaction, CH₄ can be easily oxidized to CO, resulting in decrease the CH₄ yield after 2–3 h in reaction (Fig. 6c). One should note that CO might be converted into HCHO and CH₃OH (Eqs. (9) and (10), Table 3) to promote their product yields. Meanwhile, CO can be more readily reacted with O₂ to form CO₂ (Eq. (8), Table 3). It is no surprise that this exothermic oxidation, which exhibits negative ΔH° value (-283.2 kJ mol⁻¹), is associated with highly negative ΔG° value (-257.3 kJ mol⁻¹) and, is highly thermodynamically favorable. Therefore, the CO yield dropped dramatically as reaction time goes on (Fig. 6b). Based on the knowledge of species present during the photo-reaction, a possible reaction pathway for single reaction is proposed and illustrated in Scheme 3. We suggest that CO₂ can be directly hydrogenated into several possible products, such as CH₃OH, and CH₄. On the other hand, CO can be directly produced by catalytic oxidation of CH₄. As a result, CO will react with H₂O and H₂ to produce HCHO and further favor the CH₃OH yield, respectively [28]. However, CO is easily converted to CO₂ by reacting with O₂, resulting in the decrease CO yield after 3 h in reaction (Eq. (10), Table 3). In short summary, GaN:ZnO-Ni/NiO photocatalyst successfully performs the production of H₂ and reduction of CO₂ simultaneously with an efficient catalytic activity.

3.2.3. Twin photoreactor

Due to the weather conditions changed all the time (even during a sunny day). It is impossible to have consistent results under realistic sunlight illumination. Therefore, photocatalytic CO₂ reduction in the twin photoreactor was performed under artificial sunlight, which was provided by the 300-W xenon lamp integrating with an AM1.5G filter. The light intensity in front of the twin photore-

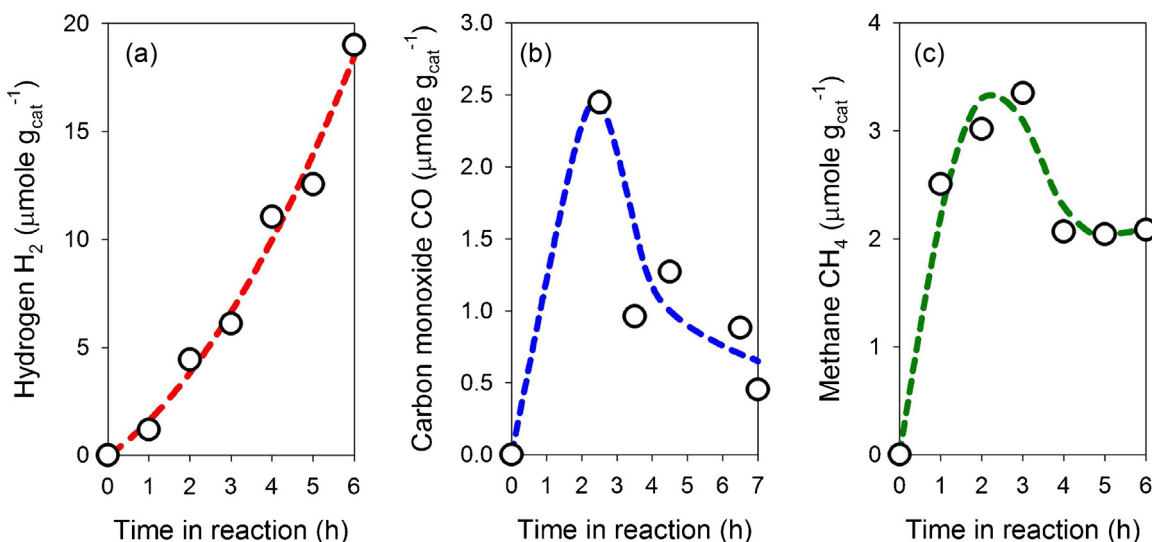
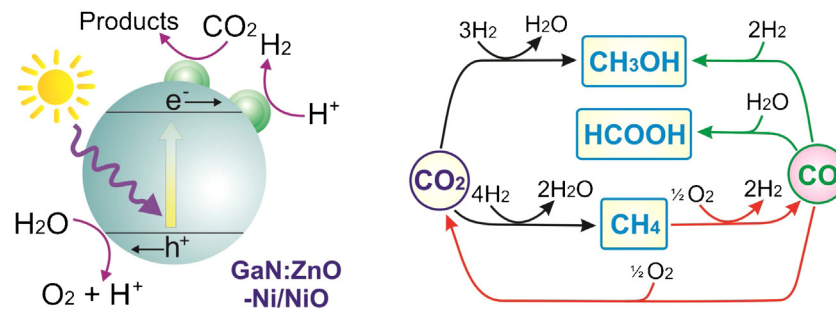


Fig. 6. The time-dependent yields of various products over GaN:ZnO-Ni/NiO photocatalyst under visible-light 300 W Xenon lamp in the single photoreactor: (a) H₂ evolution, (b) CO evolution, and (c) CH₄ evolution.



Scheme 3. The proposed diagram and reaction pathways of combined water-splitting/photo-hydrogenation over GaN:ZnO-Ni/NiO photocatalyst under visible-light 300 W Xenon lamp in the single photoreactor.

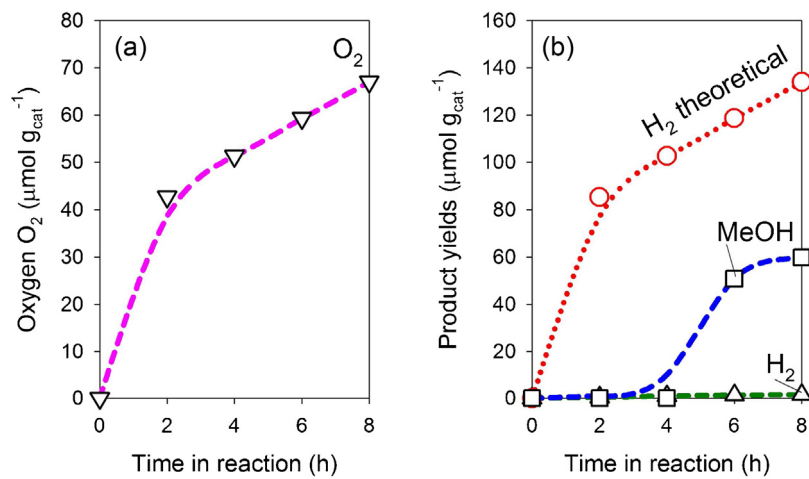


Fig. 7. The time-dependent yields of various products over GaN:ZnO-Ni/NiO photocatalyst under artificial sunlight AM1.5G 300 W Xenon lamp in the twin photoreactor: (a) O₂ evolution in left-hand compartment, (b) H₂ evolution, MeOH formation and H₂ theoretical evolution in right-hand compartment.

actor was approximately 100 mW cm⁻², which was similar to the power and spectral distribution of the realistic illumination of sun at 48.5° zenith angle. In the twin photoreactor system, both water splitting and CO₂ reduction reactions occur simultaneously. The advantage of using the twin photoreactor is that the produced O₂ and H₂-hydrocarbon products could be separated into two different compartments that can prevent either the backward reaction

between H₂ and O₂ or the oxygenation of hydrocarbon products. As a result, the generated H₂ is effectively used to photo-hydrogenate CO₂ into design products under mild conditions. Fig. 7 shows the time-dependent yields of various products over GaN:ZnO-Ni/NiO photocatalyst in the twin photoreactor under AM1.5G 300 W Xenon lamp. In the left-hand compartment, the amount of O₂ produced after 8 h of reaction is 66.96 μmol g_{cat}⁻¹ (Fig. 7a). In the right-

hand compartment, the amount of CH_3OH and H_2 produced after 8 h of reaction is 59.7 and $1.6 \mu\text{mol g}_{\text{cat}}^{-1}$, respectively (Fig. 7b). Theoretically, the amount of H_2 and O_2 produced in pure water splitting have a ratio of two-to-one [29]. Therefore, the theoretical amount of H_2 should be $134.08 \mu\text{mol g}_{\text{cat}}^{-1}$. However, only $1.6 \mu\text{mol g}_{\text{cat}}^{-1}$ of H_2 was observed in the right-hand compartment (Fig. 7b). It suggests that CH_3OH is mainly formed via the direct hydrogenation of CO_2 . It is noted that a required amount of H_2 to produce $59.7 \mu\text{mol g}_{\text{cat}}^{-1}$ of CH_3OH by direct hydrogenation is $179.1 \mu\text{mol g}_{\text{cat}}^{-1}$ which is greater than the calculated theoretical amount of H_2 ($134.08 \mu\text{mol g}_{\text{cat}}^{-1}$). Thus, some of the CH_3OH is not fully produced through the direct hydrogenation, but is also produced by the reduction of CO_2 with H_2O forming hydrocarbons [30]. Importantly, CH_3OH was found to be the major product. The reason is that the photo-hydrogenation of CO_2 to form CH_4 requires 8 photoelectrons, which is higher than that to form CH_3OH (6 photoelectrons required). In our study, visible-light (300 W Xenon lamp, 270 mW cm^{-2}), which is used to conduct single reaction, can produce more electron-hole pairs on the photocatalysts than the artificial sunlight (AM1.5G 300 W Xenon lamp, 100 mW cm^{-2}). Hence, as we observed, CH_3OH was the main product when experiment was conducted under artificial sunlight. The result is in good agreement with previous study [31]. The absence of CH_4 pathway in current condition is also attributed to the missing of HCHO .

3.2.4. Comparison of efficiency in different photoreactors

The photoreduction efficiency is compared between different photoreactors by a term called the photoreduction quantum efficiency (PQE) which was evaluated in details previously [13].

$$\text{Photoreduction quantum efficiency (\%)} = 100\%$$

$$\times (\text{number of moles of photoelectrons required for reduction} \\ \times \text{product formation rate}) / \text{incident photon rate} \quad (11)$$

To consider an competition between the reduction of H_2O to H_2 and CO_2 to CO , HCHO , CH_3OH and CH_4 ; the selectivity for CO_2 reduction based on a photoelectron basis is defined as following [32].

$$\text{Selectivity for CO}_2 \text{ reduction (\%)} = 100\%$$

$$\times (\text{No. of photoelectrons required} \times \text{CO}_2 \text{ reduction products}) / \\ \times (\text{No. of photoelectrons required} \\ \times \text{CO}_2 \text{ reduction products} + 2 \times \text{hydrogen}) \quad (12)$$

The product yields, selectivity for CO_2 reduction and QE of the single photoreactor and the twin photoreactor are summarized in Table 4. The result clearly demonstrates that twin photophotoreactor can significantly promote the photo-hydrogenation of CO_2 , even the light intensity of single reactor (270 mW cm^{-2}) is higher than that of the twin reactor (100 mW cm^{-2}). The selectivity for CO_2 reduction reaches to 99.1%. We believe that the bottleneck is the limited efficiency of the H_2 -generating; therefore, how to preferentially accelerate the producing H_2 may be a key point for further improving the activity of CO_2 photo-hydrogenation. Remarkably, the QE of the twin photoreactor is improved more than 4 folds comparing to that of the single photoreactor (an enhancement from 0.015% to 0.070%). Such significant improvement is attributed to three main reasons. Firstly, the twin photoreactor separates the O_2 and H_2 produced in each compartment, thus prevents the oxidation reaction of O_2 with the hydrocarbons generated. Furthermore, the H_2 is used immediately for the hydrogenation of CO_2 . Secondly, GaN:ZnO-Ni/NiO applied in the twin photoreactor system acts as a

Table 4

Performance comparison of the twin photoreactor and single photoreactor.

Conditions and results	Single photoreactor	Twin photoreactor
Hydrogen ($\mu\text{mol g}_{\text{cat}}^{-1} \text{h}^{-1}$)	3.16	0.20
Methane ($\mu\text{mol g}_{\text{cat}}^{-1} \text{h}^{-1}$)	0.35	ND
Methanol ($\mu\text{mol g}_{\text{cat}}^{-1} \text{h}^{-1}$)	2.24	7.46
Formaldehyde ($\mu\text{mol g}_{\text{cat}}^{-1} \text{h}^{-1}$)	0.31	ND
CO ($\mu\text{mol g}_{\text{cat}}^{-1} \text{h}^{-1}$)	0.07	ND
Selectivity for CO_2 photoreduction (%)	73.6	99.1
PQE (%)	0.015	0.070
Light sources	300 W Xenon lamp: 270 mW cm^{-2}	AM1.5G 300 W Xenon lamp: 100 mW cm^{-2}

Note: ND—not detected; QE—photoreduction quantum efficiency; the product ($\mu\text{mol g}_{\text{cat}}^{-1} \text{h}^{-1}$) is an average rate of batch reaction in 6 or 8 h.

dual-function visible-light photocatalyst, which provides the ability to reduce CO_2 via the produced H_2 . The photocatalytic reaction is enhanced because hydrogenation of CO_2 is thermodynamically favorable and is a spontaneous reaction. Last but not least, IO_3^-/I^- was incorporated in the twin photoreactor for the first time. Due to the shuttle redox mediator, the energy barrier for water splitting and reduction of CO_2 was diminished, resulting in a higher QE.

4. Conclusions

In summary, H_2O water-splitting and CO_2 photo-hydrogenation are successfully explored and adopted by using the twin photoreactor system. Our present work has demonstrated that GaN:ZnO-Ni/NiO and Pt/WO_3 photocatalysts can significantly enhance the efficient photocatalytic water splitting and hydrogenation. GaN:ZnO-Ni/NiO photocatalyst reduces CO_2 via the produced H_2 while Pt/WO_3 photocatalyst produces O_2 simultaneously in each compartment of twin photoreactor. Additionally, IO_3^-/I^- is incorporated in the twin photoreactor for the first time to balance charge. Applying twin photoreactor can improve significantly QE more than 4 folds from 0.015% to 0.070%, in compared with single photoreactor, with the same photocatalyst. Moreover, the selectivity for CO_2 reduction in the twin photoreactor reaches to 99.1% which is higher than that in the single photoreactor (73.6%). Despite the prominent results achieved, there is a need for further improving the efficiency of photocatalytic CO_2 hydrogenation. The bottleneck is obviously the limited efficiency of the H_2 -generating. Therefore, the goal toward solving global warming and energy crisis will be one step closer if a high-efficient photocatalyst is discovered in the future and applied to the twin photoreactor system.

Acknowledgements

This work was financially supported by the Taiwan Ministry of Science and Technology under the project NSC 101-2621-M-002-012, and was also financially supported by the NSFC (Grant U1305242). In addition, we appreciated the Taiyen Tongsiao Factory for providing Neosepta membrane.

Appendix A. Supplementary data

Supplementary data associated with this article can be found, in the online version, at <http://dx.doi.org/10.1016/j.apcata.2015.08.027>.

References

- [1] A. Creamer, B. Gao, Overview of Greenhouse Gases and Global Warming, Carbon Dioxide Capture: An Effective Way to Combat Global Warming, Springer International Publishing, 2015, pp. 1–15.
- [2] N. Armaroli, V. Balzani, *Angew. Chem. Int. Ed.* 46 (2007) 52–66.
- [3] C.S. Jeffrey, Developments and Innovation in Carbon Dioxide (CO_2) Capture and Storage Technology, in: M.M. Maroto-Valer (Ed.), Woodhead Publishing, 2010, pp. 463–501.
- [4] T. Inoue, A. Fujishima, S. Konishi, K. Honda, *Nature* 277 (1979) 637–638.
- [5] K. Li, X. An, K.H. Park, M. Khraisheh, J. Tang, *Catal. Today* 224 (2014) 3–12.
- [6] A.D. Handoko, K. Li, J. Tang, *Curr. Opin. Chem. Eng.* 2 (2013) 200–206.
- [7] Y. Kohno, H. Ishikawa, T. Tanaka, T. Funabiki, S. Yoshida, *Phys. Chem. Chem. Phys.* 3 (2001) 1108–1113.
- [8] Y. Kohno, T. Tanaka, T. Funabiki, S. Yoshida, *Phys. Chem. Chem. Phys.* 2 (2000) 2635–2639.
- [9] Y. Kohno, T. Tanaka, T. Funabiki, S. Yoshida, *Chem. Commun.* (1997) 841–842.
- [10] K. Teramura, T. Tanaka, H. Ishikawa, Y. Kohno, T. Funabiki, *J. Phys. Chem. B* 108 (2004) 346–354.
- [11] H. Ahmad, S.K. Kamarudin, L.J. Minggu, M. Kassim, *Renew. Sust. Energy Rev.* 43 (2015) 599–610.
- [12] R. Abe, K. Sayama, K. Domen, H. Arakawa, *Chem. Phys. Lett.* 344 (2001) 339–344.
- [13] W.-H. Lee, C.-H. Liao, M.-F. Tsai, C.-W. Huang, J.C.S. Wu, *Appl. Catal. B* 132–133 (2013) 445–451.
- [14] Y. Kohno, T. Tanaka, T. Funabiki, S. Yoshida, *Phys. Chem. Chem. Phys.* 2 (2000) 5302–5307.
- [15] S. Ichikawa, *Energy Convers. Manage.* 36 (1995) 613–616.
- [16] K. Teramura, S.-i. Okuoka, H. Tsuneoka, T. Shishido, T. Tanaka, *Appl. Catal. B* 96 (2010) 565–568.
- [17] K. Teramura, H. Tsuneoka, T. Shishido, T. Tanaka, *Chem. Phys. Lett.* 467 (2008) 191–194.
- [18] K. Maeda, K. Teramura, T. Takata, M. Hara, N. Saito, K. Toda, Y. Inoue, H. Kobayashi, K. Domen, *J. Phys. Chem. B* 109 (2005) 20504–20510.
- [19] K. Maeda, K. Domen, *Chem. Mater.* 22 (2010) 612–623.
- [20] K. Maeda, T. Takata, M. Hara, N. Saito, Y. Inoue, H. Kobayashi, K. Domen, *J. Am. Chem. Soc.* 127 (2005) 8286–8287.
- [21] K. Maeda, K. Teramura, K. Domen, *Catal. Surv. Asia* 11 (2007) 145–157.
- [22] T. Takata, K. Shinohara, A. Tanaka, M. Hara, J.N. Kondo, K. Domen, *J. Photochem. Photobiol. A* 106 (1997) 45–49.
- [23] C.-H. Liao, C.-W. Huang, J.C.S. Wu, *Catalysts* 2 (2012) 490–516.
- [24] Y.-T. Wu, Y.-H. Yu, V.-H. Nguyen, K.-T. Lu, J.C.-S. Wu, L.-M. Chang, C.-W. Kuo, *J. Hazard. Mater.* 262 (2013) 717–725.
- [25] M.A. Peck, M.A. Langell, *Chem. Mater.* 24 (2012) 4483–4490.
- [26] C.D. Wagner, G.E. Muilenberg, *Handbook of X-ray Photoelectron Spectroscopy: a Reference Book of Standard Data for Use in X-ray Photoelectron Spectroscopy*, PerkinElmer Corp., Physical Electronics Division, Eden Prairie, Minn, 1979.
- [27] Xiaoding, J.A. Moulijn, *Energy Fuels* 10 (1996) 305–325.
- [28] Y.-H. Cheng, V.-H. Nguyen, H.-Y. Chan, J.C.S. Wu, W.-H. Wang, *Appl. Energy* 147 (2015) 318–324.
- [29] C.-C. Lo, C.-W. Huang, C.-H. Liao, J.C.S. Wu, *Int. J. Hydrogen Energy* 35 (2010) 1523–1529.
- [30] H. Yamashita, Y. Fujii, Y. Ichihashi, S.G. Zhang, K. Ikeue, D.R. Park, K. Koyano, T. Tatsumi, M. Anpo, *Catal. Today* 45 (1998) 221–227.
- [31] P.-Y. Liou, S.-C. Chen, J.C.S. Wu, D. Liu, S. Mackintosh, M. Maroto-Valer, R. Linforth, *Energy Environ. Sci.* 4 (2011) 1487–1494.
- [32] Q. Zhai, S. Xie, W. Fan, Q. Zhang, Y. Wang, W. Deng, Y. Wang, *Angew. Chem. Int. Ed.* 52 (2013) 5776–5779.